LOCAL THERMAL AND STRUCTURAL BEHAVIOR OF CONCRETE AT ELEVATED TEMPERATURES

E. L. GLUEKLER

General Electric Co., Advanced Reactor Systems Department, 310 DeGuigne Drive, Sunnyvale, California 94086, U.S.A.

At elevated temperatures, structural responses of surface heated concrete walls are significantly affected by the release of capillary, adsorbed and chemically bound water. Two major phenomena are generally observed: (1) degradation of concrete strength because of the loss of hydraulic bonds in gelatious, hydrated compounds, shrinkage of the cement matrix, increase in porosity and microcracking, and (2) pressurization of concrete pores because of vaporization of water and expansion of gases.

Under certain conditions, the combined effects of material degradation and internal pressurization could lead to crack formation parallel to the surface, or spallation. This failure mode has been observed in some experiments, but not consistently. In this paper, a criterion for concrete spallation is described which depends on (1) loading conditions including pore pressures and thermal stresses, and (2) materials characteristics at elevated temperatures.

The internal pressurization of concrete arises from the evaporation of water and expansion of gases contained in the pores. Water in concrete exists in various forms as free or capillary water, adsorbed water and chemically bound water; each component is given off at characteristic temperatures. Based on a concrete heat and mass transfer model that treats filtration and diffusion, evaporation and condensation, the pressure distribution in the concrete was determined for a range of assumed conditions and material properties. It was found that peak pressures on the order of 2 to 7 atm occur at an evaporation front which separates a cold, wet zone from a hot, dessicated zone. The evaporation front advanced into the concrete as surface heating was maintained, with little variation of the peak pressure. The calculation of mass transport and pore stresses was based on an open pore model. The existence of such an open pore structure was verified by electron microscope investigations of small specimens exposed to various temperatures.

To describe local fracture characteristics of concrete structures, a failure surface was defined in terms of the uniaxial tensile and compressive strength of a cylinder and the biaxial compressive strength. The failure surface was approximated by a generalized cone with a parabolic contour centered along the average axis of all principal stresses. Although significant uncertainties still exist, it was concluded that spallation failure of surface heated concrete would occur only under very rapid heating to high surface temperatures (> 400°C) and a high content of evaporable water or a low permeability.

1. Introduction

Local failures at the surface of concrete structures (spallation) and significant water release have been observed when surfaces were exposed to elevated temperatures as for instance in building fires. In liquid metal fast breeder reactors, spillage of hot sodium onto concrete structures could potentially cause such failures, and the release of water could result in selfsustaining, exothermic chemical reactions between sodium, water and solid concrete constituents, if adequate protection were not available. To provide sufficient safety information for the design of reactor containment cells, a program was initiated at General Electric Company with the intent of developing tools for the evaluations of potential material interactions and associated containment responses. Results obtained from this work pertaining to the behavior of concrete microstructure at elevated temperatures, water release characteristics and surface failure are presented in this paper.

2. Changes in Microstructure and Properties at Elevated Temperatures

2.1 Formation of Phases and Decomposition

Concrete, in general, is produced from a mixture of aggregate, sand, cement and water. After addition of water to the cement, a consolidation process occurs leading to the formation of a rigid interlocking matrix of hydration products, which gradually consume most of the available water. First, a gel coating of the sand and aggregate particles develops consisting mainly of calcium silicate hydrate, and small fibers and platelike crystals of CaOH appear. The fibers form an interwoven mesh that consolidates to create a rigid crystalline structure of the tobermorite type, or $[Ca_5Si_6O_{16}(OH)_2]\cdot 2H_2O$, with CaOH laminations. The hardened paste is strongly hydrophilic and porous with a typical porosity of 0.40 to 0.55. Scanning electron microscopy examinations indicated an open, interconnected pore structure with pore sizes between 0.1 and 20 µm at room temperature (see Figures 1 and 2). The presence of fibers extending locally into the pores indicates the initial existence of capillary water. The surface of cast samples showed irregular shrinkage cracks approximately 2 µm wide.

The major fraction of water in concrete (approximately 50 percent) is chemically combined as hydroxides by covalent or by hydrogen bonds. The hydration reaction usually does not go to completion. This is demonstrated by the generally known fact that hardened and aged cement, when ground and mixed with water, develops some strength again. Since most of the products of hydration are colloidal, the surface area of the solid phase increases enormously during the hydration, and free water becomes adsorbed on this surface. Some water is also retained as interlayer water, bound by strong forces arising from active sites on the adsorbent, which leads to the formation of definite orientations of water molecules. If the initial water to cement ratio exceeds 0.4, capillary or free water is expected in the pores. For smaller ratios, the paste would become completely desiccated, and some fraction of the cement may remain unhydrated.

Differential Thermal Analysis (DTA) [1, 2, 3] and heating tests with small samples [4] provided a good understanding of phase decompositions and transformations and associated changes in moisture distribution at elevated temperatures. Upon heating to 100°C, the capillary water is evaporated and released. The loss of adsorbed water occurs over a wide temperature range. However, all evaporable water should be given off at 300°C. At this temperature, some changes appear in the microstructure such as the formation of fibrous, columnar phases, but no significant changes are apparent in the pore and microcrack distributions.*

The decomposition of $Ca(OH)_2$ into CaO at temperatures between 500 and 600^{o}C is expected to result in volumetric shrinkage of about 44 percent causing a considerable increase in porosity. Indeed, the samples heated to 600^{o}C showed wide shrinkage and surface cracks and were very brittle. Although no changes occurred in the aggregate, the small-grain interstitial structure appeared less cohesive with reduced strength. No attempt was made to quantify porosity changes based on microstructural investigations, however, quantitative estimates were obtained from data reported for preheating of refractory concrete consisting of Portland cement and bricks [5]. From these data, it was inferred that porosity increases approximately linearly by almost 40 percent during the heating from room temperature to 600^{o}C. Above this temperature, no further change was noted until at the sintering temperature the porosity diminishes. The heating of small samples to 900^{o}C produced very brittle, crumbly material. The surface showed more and wider shrinkage cracks than at lower temperatures, and the interstitial structure exhibited the first signs of sintering and rounded shapes of particles, with microporosity between them. The dehydration of calcium silicate hydrate is complete at 900^{o}C and some wollastonite, $CaSiO_3$, should have formed. Below 800^{o}C, changes in the concrete appear to be independent of the aggregate and are essentially determined by the behavior of the cement phase.

2.2 Water Release Characteristics

The investigation of concrete samples at elevated temperatures indicated that cement has a relatively low degree of chemical stability and significant amounts of water are released. The processes and amounts of water release are notably different for temperatures below and above the boiling point of water. In the low temperature range (less than 105^{o}C), water emission is controlled by diffusion processes caused by concentration gradients [6]. At higher temperatures, moisture transport was found to be controlled by filtration under pressure gradients [7]. To determine water release characteristics for a wide range of surface temperatures, and pressure distributions as input to structural response evaluations, a comprehensive diffusion - filtration model was developed based on thermodynamic principles.

The governing continuity, energy, and momentum equations for the heat and mass transport processes are:

A. Continuity

$$\sum_{i=1}^{2}\left[\varepsilon\frac{\partial(S_i\rho_i)}{\partial t} + \frac{\partial}{\partial x}(u_i\rho_i + j_i)\right] = 0 \tag{1}$$

$$\varepsilon\frac{\partial(S_3\rho_3)}{\partial t} + \frac{\partial}{\partial x}(u_3\rho_3 + j_3) = 0 \tag{2}$$

where S_i and ρ_i represent the volume fraction and density of the ith component within the pores (i = 1, water; 2, water vapor; 3, air), ε = concrete porosity, t = time, x = spatial coordinate, $u_2 = u_3$ = mass average velocity of gas mixture.

B. Energy

$$\sum_{i=1}^{3}\left\{\varepsilon\frac{\partial(S_i\rho_i e_i)}{\partial t} + \frac{\partial}{\partial x}\left[(j_i + u_i\rho_i)h_i\right]\right\} +$$

*To maximize thermo-mechanical effects, concrete samples were inserted into a preheated oven.

$$+ (1 - \varepsilon)\rho_o \left\{ \frac{\partial e_o}{\partial t} - \left[h_d(T) + h_{fg} \right] \frac{\partial m_n}{\partial t} \right\} = \frac{\partial}{\partial t} \left(K \frac{\partial T}{\partial x} \right) \tag{3}$$

where T = temperature, e = specific internal energy, h = specific enthalpy, K = thermal conductivity, h_d = decomposition energy of hydration products, h_{fg} = latent heat of vaporization at constant volume, m_n = mass of nonevaporable water per unit volume, and the subscript o denotes solid material.

C. Momentum - The momentum equation is represented by the equations of motion under filtration (Darcy's law) and diffusion:

$$\vec{u} = \frac{\kappa(S,T)}{\mu} \nabla p \quad \text{and} \quad j_i = -D(S) \frac{\partial \omega_i}{\partial x} \tag{4,5}$$

where p = pressure, κ = permeability, μ = viscosity, ω_i = mass fraction of the i^{th} specie, D = diffusion coefficient.

The evaporation of capillary water can be based on the assumption of local thermodynamic equilibrium and the Clausius-Clapeyron equation. The dehydration reactions can be described as first order mechanisms. Based on the absolute-rate-reaction theory, the rate of weight loss is

$$\frac{d}{dp} (\Delta w) = \left[w_n(T) - \Delta w \right] \frac{kT}{h} \exp \left(- \frac{\Delta F}{RT}\right) \tag{6}$$

where Δw = weight change, w_n = mass of nonevaporable water, k = Boltzmann constant, h = Planck constant, ΔF = free energy of activation, R = gas constant. The source term for nonevaporable water, m_n, can be expressed in terms of $w_n(T)$.

An explicit numerical solution with specific treatment of the wet and dry zones was used to determine typical pressure, temperature, and moisture distributions, and water release rates. Figures 3 and 4 show the pressure distribution and water release rate as a function of time for a surface temperature of 400^oC. Figure 3 indicates the rate of advance of the evaporation front.
The peak pressure occurs at the evaporation front, and water is transported to both the hot surface and to the cold zone where it recondenses, creating a higher apparent heat transfer coefficient for the cold side near the evaporation front.

3. Local Loading Conditions

3.1 Pore Stresses

Maximum pore pressures on the order of 2 to 7 atm were calculated with the filtration-diffusion model. This is in good agreement with preliminary experimental results [8]. Evaluations with the model indicated that the peak pressure appears to be relatively insensitive to variations in thermal conductivity, surface temperatures (above 100^oC), species diffusion coefficient and total porosity, but it seems to depend strongly on Darcy's coefficient and permeability which in turn depends on temperature or dehydration shrinkage and pore saturation with evaporable water. Some authors claim that the assumption of local thermodynamic equilibrium would give peak pressures in excess of 1000 atm [9,10], which was recognized as being incorrect. The present diffusion-filtration model does not substantiate such claims.

A large fraction of the space initially filled with water will become occupied by gel which forms during the consolidation process and expands to 2.1 times the volume of the unhydrated cement. The gel itself has a permeability on the order of 7×10^{-14} cm/s which is a factor of 20 to 100 less permeable than the cement paste as a whole [11], i.e., the flow resistance should be controlled by interconnected capillary pores and cracks in the cement paste. In the present experiments this was found to produce cracks larger than the "average" capillary diameter.

Some discrepancies exist in the literature regarding the change of permeability with temperature. While some sources [9,10] indicate a rapid increase of permeability at $100^{\circ}C$ and almost temperature independence above $150^{\circ}C$, the trend of other sources would imply a continuous increase up to $600^{\circ}C$, because the permeability increases with porosity [11] which in turn increases with temperature [5]. Additional permeability investigations with well characterized concrete samples (e.g., measurement of initial water content) and heating conditions are required to resolve the difference in interpretations.

The pore pressure distributions shown in Figure 3 were calculated based on a temperature independent permeability of 10^{-11} cm^2. The pore stresses, σ_p, caused by a pore pressure $p(x)$ at a location x from the surface, can be determined assuming a model for an open pore structure with a total porosity, ε. This model is illustrated in Figure 5. The interconnected capillary pores were divided into three components in the direction of the principal stresses. The pore stresses are then determined from

$$\sigma_{pi}(x) = p(x) \left[4\sqrt{\frac{\varepsilon + \varepsilon_s(T,x)}{3\pi}} + \frac{\varepsilon + \varepsilon_s(T,x)}{3}) \ \alpha_i \right] \tag{7}$$

where α_i = index = 0 for $i = 2, 3$; ε_s = porosity increase because of dehydration shrinkage. For $\alpha = 1$, the shear stresses on the capillary walls perpendicular to surface are taken into account. The stresses were found to be independent of the pore size distribution. It is not necessary to include stress concentration factors in the pore stress model since the effective stress is compared with failure surface values, which include stress concentration effects implicitely.

3.2 Thermal Stresses

Surface heated concrete structures experience temperature gradients and compressive stresses in the hot surface layer. In the tension-compression stress regime considered, the equilibrium condition can be expressed in terms of elastic displacements

$$\frac{\partial e}{\partial x_i} + (1 - 2\nu)\nabla^2 \xi_i = 2(1 + \nu)(\alpha - \alpha_s) \frac{\partial T}{\partial x_i} \tag{8}$$

where $e = (1 - 2\nu)\sigma_{i,i}/E$, ν = Poisson's ratio, σ_i = principal stress components, α = coefficient of thermal expansion, α_s = shrinkage coefficient, ξ_i = displacement components in the direction x_i of σ_i; the second index i denotes the summation of i components. Thermal stress distributions can be obtained from a solution of the displacement components using elastic stress-strain correlations. For long term exposure to elevated temperatures, it may be necessary to consider creep relaxation effects of stresses [12]. Since sufficient applicable information is not available for creep characteristics in the presence of internal pressure, water release, and dehydration, this effect was neglected in the present evaluation.

4. Failure Modes

4.1 Failure Surface Model

The strength of concrete arises from two kinds of cohesive bonds: (1) physical attraction, or van der Waals' forces, between surfaces and (2) cohesion by chemical bonds which are much stronger than the van der Waals' forces, but cover only a small fraction of the surface of gel particles. At elevated temperatures, the structural behavior of concrete is significantly affected by microstructural changes as described in Section 2.1. Several mechanisms including dehydration (loss of chemical bonds), decomposition of $Ca(OH)_2$, micro-cracking caused by shrinkage of cement matrix, and differential thermal expansion between aggregate and cement, lead to a degradation of structural properties resulting in an almost complete loss of strength above 600^oC.

The considerable difference between the tensile and compressive strength of concrete requires a more general failure criterion than for metals where a failure or yield criterion is employed that is independent of the hydrostatic pressure. A concrete failure criterion was selected which is described by a failure surface that depends on I_1 and I_2, where I_1 and I_2 are the first and second invariants of the stress tensor. The failure surface was assumed to be symmetric to the average principal stresses, although the assumption of a circular cross section is only valid for failures resulting from perfectly isentropic phenomena (Failures with anisotropic causes would produce triangular like cross sections with vertices on the principal stress axes, see Figure 6). The failure surface following the approach by Saugy [13] is

$$A(\beta_c, n, \gamma) = \sum_j \tau_j (I_2^{*\frac{1}{2}} - E)^j - I_1^* = 0 \qquad (9)$$

where β_c = uniaxial compressive strength of a cylinder, $n\beta_c$ = biaxial compressive strength, $\gamma\beta_c$ = uniaxial tensile strength, τ, E = stress dependent variables. To obtain estimates for the local failure characteristics of surface heated concrete, additional simplifications and assumptions were introduced: (1) close to the heated structural surface, only the tensile - compressive portion of the failure surface is of interest, (2) in this regime, failure is by a single cleavage crack with a linear stress-strain relation up to failure, (3) the contour of the failure surface was assumed to be parabolic, and (4) the meridians of the failure envelope intersect the axis of symmetry at an angle of 45^o. Assumptions (2), (3) and (4) seem to be supported by experimental data [14]. If the loading consist of thermal stresses σ_{th} and pore stresses σ_p, and $\sigma_p << \sigma_{th}$ (in accordance with $\gamma << n$), the failure condition can be described as

$$\frac{\sigma_{th}^2 - 2\,\sigma_{th}\sigma_p}{\beta_c^2 (n + \gamma)^2 (1 - \frac{\sigma_p}{\gamma\beta_c})} \geq 1 \qquad (10)$$

4.2 Failure Evaluation

A preliminary evaluation of the failure criterion showed that failure of heated concrete surface occurs most likely by crack formation parallel to the hot surface. This phenomenon is generally known as spallation. Based on the criterion it can be concluded that concrete spallation would occur only under extreme conditions such as a high surface temperature ($\sim 400^oC$) combined with a high water content and low permeability. This is in agreement with experimental observations [15]. Spallation cracks were observed at a depth of 1.5 to 2.5 cm from the surface consistent with predictions with the filtration-diffusion model for water release, which indicates a peak pore pressure at this depth. Figure 7 illustrates a spallation crack schematically. Spallation conditions for combinations of σ_{th}, σ_p and temperature T are given in Figure 8. It should be noted that the maximum allowable pressure is significantly reduced by the thermal stresses as σ_{th} approaches the crushing limit.

5. Concluding Remarks

Mechanistic models were developed for predicting water release from concrete and local failure characteristics. The filtration-diffusion model for water release showed good agreement with preliminary experimental results for short times. Additional experiments need to be performed with well characterized samples for a range of surface temperatures to verify the general applicability of the model. The concrete failure criterion indicated that for a range of conditions, spallation could occur. Although this phenomenon has been observed in experiments and building fires, well defined experiments with appropriate characterization of the Young's modulus, thermal expansion, permeability, initial water content, and structural properties are lacking. Such experiments would be required to verify the failure model.

Acknowledgement

Work in the subject area was performed under Contract EY-76-C-03-0893 of the U.S. Department of Energy. The author would like to thank Dr. A. Dayan, Tel-Aviv University, and P. Yin of General Electric Company, for their significant contributions in developing a model for water release from concrete.

References

[1] PETZOLD, A. and GÖHLERT, I., Tonindustrie Zeitung, 86, 10 (1962).

[2] PEEHS, M. and DÖRR, W., "Physical Properties and Behavior of Heated Basaltic Concrete," PAHR Information Exchange Meeting, ANL, November 2-3, 1977, ANL-78-10.

[3] Light Water Reactor Safety Research Program, Quarterly Report, January - March 1976, Sandia Laboratories, SAND-76-0369, September, 1976.

[4] Advanced Safety Analysis, Thirteenth Quarterly Report, September - November 1977, General Electric Company, GEFR-14038 - 13, December, 1977.

[5] GIBBELS, H., "Feuerfester Beton auf Basis des Unterwellenborner Hochofenzements," Diploma Thesis, Weimar, 1960.

[6] MCDONALD, J.W., "Moisture Migration in Concrete," ORNL-TM-5051, 1975.

[7] ENGLAND, G.L., "Migration of Moisture and Pore Pressure in Heated Concrete," First Int. Conf. Structural Mechanics in Reactor Technology, Berlin, Germany, 1971, Paper # 2/4.

[8] POSTMA, A.K., MCCORMACK, J.D., SCHUR, J.A., "A Study of Water and Gas Release From Heated Concrete," Hanford Engineering Development Laboratory, HEDL-TC-996, December, 1977.

[9] BAŽANT Z.P. and THONGUTHAI, W., "Pore Pressure and Drying of Concrete at High Temperatures," Department of Civil Engineering, Northwester University, Evanston, IL, Structural Engineering Report 77-8/640/5, August, 1977.

[10] BAŽANT, Z.P., "Thermal Effects, Creep and Nonlinear Response of Concrete Reactor Vessels," Anais da conferência sobre análise, projeto e construção des estruturas de centrais nucleares, Porto Alegre, Brasil, April, 1978.

[11] POWERS, T.C., "Structure and Physical Properties of Hardened Portland Cement Paste," J. Americ. Ceram. Soc., 41, pp. 1-6, January, 1978.

[12] HUBER, G., "Concrete - The Maturity of a Reactor Material," Conf. Nucl. Energy Maturity, Paris, 1975.

[13] SAUGY, B., "Contribution à l'étude théorique du comportement nonlinéaire des structures massives en beton sous charges rapides," Bulletin techn. de la Suisse romande, 22, 1969.

[14] KUPFER, H., HILSDORF, H.K., and RUSCH, H., "Behavior of Concrete Under Biaxial Stresses," J. Americ. Concrete Institute, 66, (8), August, 1969.

[15] HARGREAVES, K., "Sodium Fires," TRG Memo - 6760(R), December, 1974.

Figure 1: Concrete Microstructure at Room Temperature (Magnefied 5000X)

Figure 2: Concrete Microstructure at Room Temperature (Magnefied 5000X)

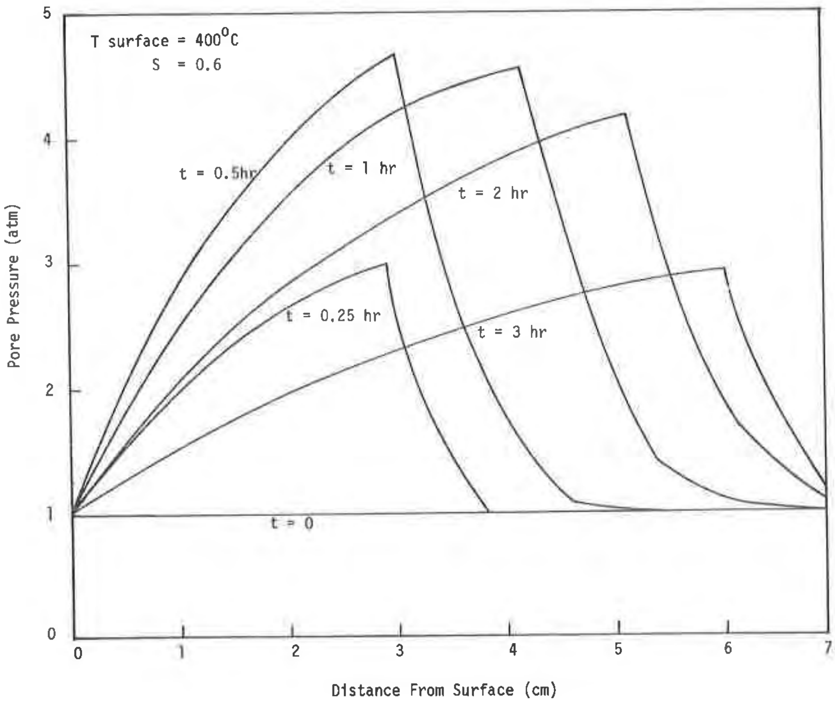

Figure 3: Transient Pressure Response

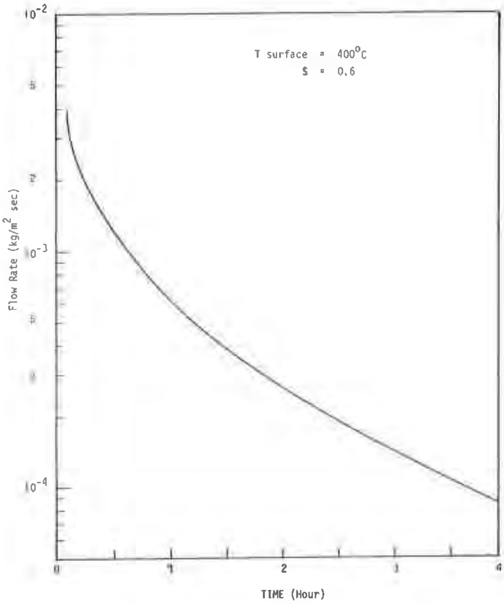

Figure 4: Rate of Water Vapor Release From Concrete

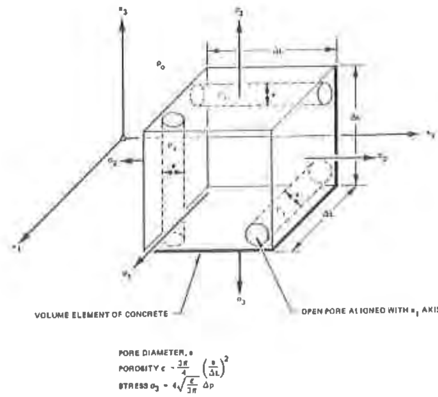

Figure 5: Pore Stress Model

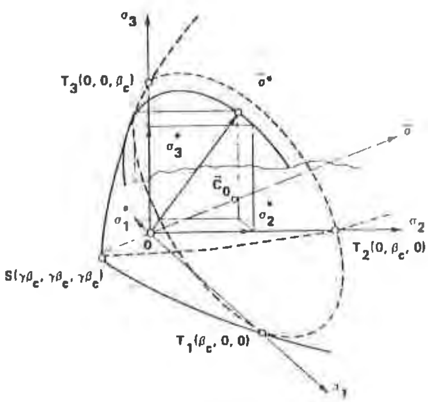

Figure 6: Fracture Surface Model

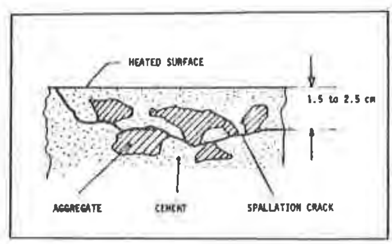

Figure 7: Spallation Crack (Schematic)

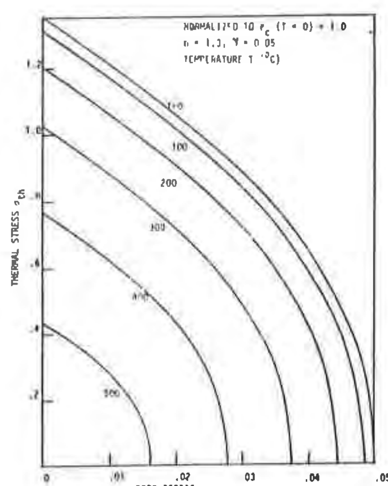

Figure 8: Local Concrete Failure Conditions